TABLE I. Values of the probabilities for coincidence observation of positronium annihilation photons of various combinations of polarizations. The photons pass through magnetic channels with the magnetic field directions indicated by + or − below, corresponding to fields pointing to the right or left in Fig. 1.

	$P(u_1^a,u_1^b)=P(u_2^a,u_2^b)$	$P(u_1^a,u_2^b)=P(u_2^a,u_1^b)$
$H_a=H_b=+$, equivalent to $H_a=H_b=-$	$\frac{1}{8}[\exp(-\lambda_- t_a-\lambda_+ t_b)-\exp(-\lambda_+ t_a-\lambda_- t_b)]^2$	$\frac{1}{8}[\exp(-\lambda_- t_a-\lambda_+ t_b)+\exp(-\lambda_+ t_a-\lambda_- t_b)]^2$
$H_a=+$, $H_b=-$, equivalent to $H_a=-$, $H_b=+$	$\frac{1}{8}[\exp(-\lambda_-(t_a+t_b))-\exp(-\lambda_+(t_a+t_b))]^2$	$\frac{1}{8}[\exp(-\lambda_-(t_a+t_b))+\exp(-\lambda_+(t_a+t_b))]^2$
$H_a=0$, $H_b=\pm$, equivalent to $H_a=\pm$, $H_b=0$	$\frac{1}{8}e^{-2\lambda t_a}[\exp(-\lambda_\pm t_b)-\exp(-\lambda_\mp t_b)]^2$	$\frac{1}{8}e^{-2\lambda t_a}[\exp(-\lambda_\pm t_b)+\exp(-\lambda_\mp t_b)]^2$
$H_a=0$, $H_b=0$	0	$\frac{1}{2}\exp(-2\lambda(t_a+t_b))$

respectively, of the Compton scattering cross section.[8] Once again we see the striking result that the observations are correlated. The coincidence rate considered above is zero for equal lengths of magnetized iron ($t_a=t_b$) and depends quadratically on (t_a-t_b) for small differences in length.

Not only does the experiment proposed here seem feasible, but in addition the properties of the absorbing medium are under our control. This is in contrast to the K^0-meson case, where the "absorbing" properties of the vacuum are fixed. In particular, one can look at several arrangements for the directions of the magnetic fields in the iron absorbers, and in so doing get quite different results for the coincidence probabilities of Eq. (5). These various possibilities are summarized in Table I, where the direction of the magnetic fields is indicated as + or − for fields pointing right or left in Fig. 1. In the table, $\lambda=\frac{1}{2}Nc\sigma_0 Z$. It is seen from Table I that reversing the field in one of the pieces of iron changes the response for the two photons in the same way that starting with $C=+1$ compared to starting with $C=-1$ changes the response for the K^0 case.

It would seem, then, that one could demonstrate in a straightforward and dramatic manner than when two particles like $K^0-\bar{K}^0$ or 2γ are created simultaneously, the probabilities involved in observing any further events related to their simultaneous creation must be calculated quantum-mechanically and are correlated, even for macroscopic distances in absorbing media.

[8] See Fagg and Hanna, reference 5, Eqs. II 8–10, III 5.

ACKNOWLEDGMENT

We would like to thank Professor J. S. Toll for an interesting discussion.

PHYSICAL REVIEW VOLUME 121, NUMBER 4 FEBRUARY 15, 1961

Heavy Nuclei in the Primary Cosmic Radiation at Prince Albert, Canada. II*

H. AIZU,† Y. FUJIMOTO, S. HASEGAWA, M. KOSHIBA,‡ I. MITO,§ J. NISHIMURA, AND K. YOKOI§
Institute for Nuclear Study, University of Tokyo, Tanashi, Tokyo, Japan

AND

MARCEL SCHEIN‖
Department of Physics, Enrico Fermi Institute for Nuclear Studies, University of Chicago, Chicago, Illinois

(Received August 19, 1960; revised manuscript received November 4, 1960)

The investigation of the low-energy primary cosmic radiation has been extended to include the heavier elements of $Z\geq 9$: Sec. 1; the light elements of Li, Be, and B: Sec. 2; and α particles: Sec. 3. The results of a previous paper on carbon, nitrogen, and oxygen have also been confirmed with better statistics. The energy spectra of all these components show a general similarity in shape. A possible deviation of the light-element spectrum from this similarity is discussed. The abundances of various elements in the low-energy region of 200 to 700 Mev per nucleon are essentially the same as observed in the higher energy region.

1. THE HEAVIER ELEMENTS OF $Z\geq 9$

THE charges and energies of the heavy nuclei in the primary cosmic radiation have been determined from the analysis of the tracks recorded by them in the stack of photographic emulsions.

A detailed description of the assembly, exposure, and processing of the stack has been given in Sec. 2 of Part I.[1]

The scanning for the heavier elements has been per-

* This work has been supported in part by the U. S. Committee of IGY, the National Science Foundation, and a joint program of the Office of Naval Research and the U. S. Atomic Energy Commission.

† Department of Physics, Rikkyo University, Tokyo, Japan; now at Department of Physics, Northwestern University, Evanston, Illinois.

‡ Now at Department of Physics, University of Chicago, Chicago, Illinois; on leave of absence from University of Tokyo, Tokyo, Japan.

§ College of General Education, University of Tokyo, Komaba, Tokyo, Japan.

‖ This paper was completed after the death of Professor Marcel Schein. Therefore, the responsibility for any possible error in this paper rests on the other authors.

[1] H. Aizu, Y. Fujimoto, S. Hasegawa, M. Koshiba, I. Mito, J. Nishimura, K. Yokoi, and M. Schein, Phys. Rev. **116**, 436 (1959).

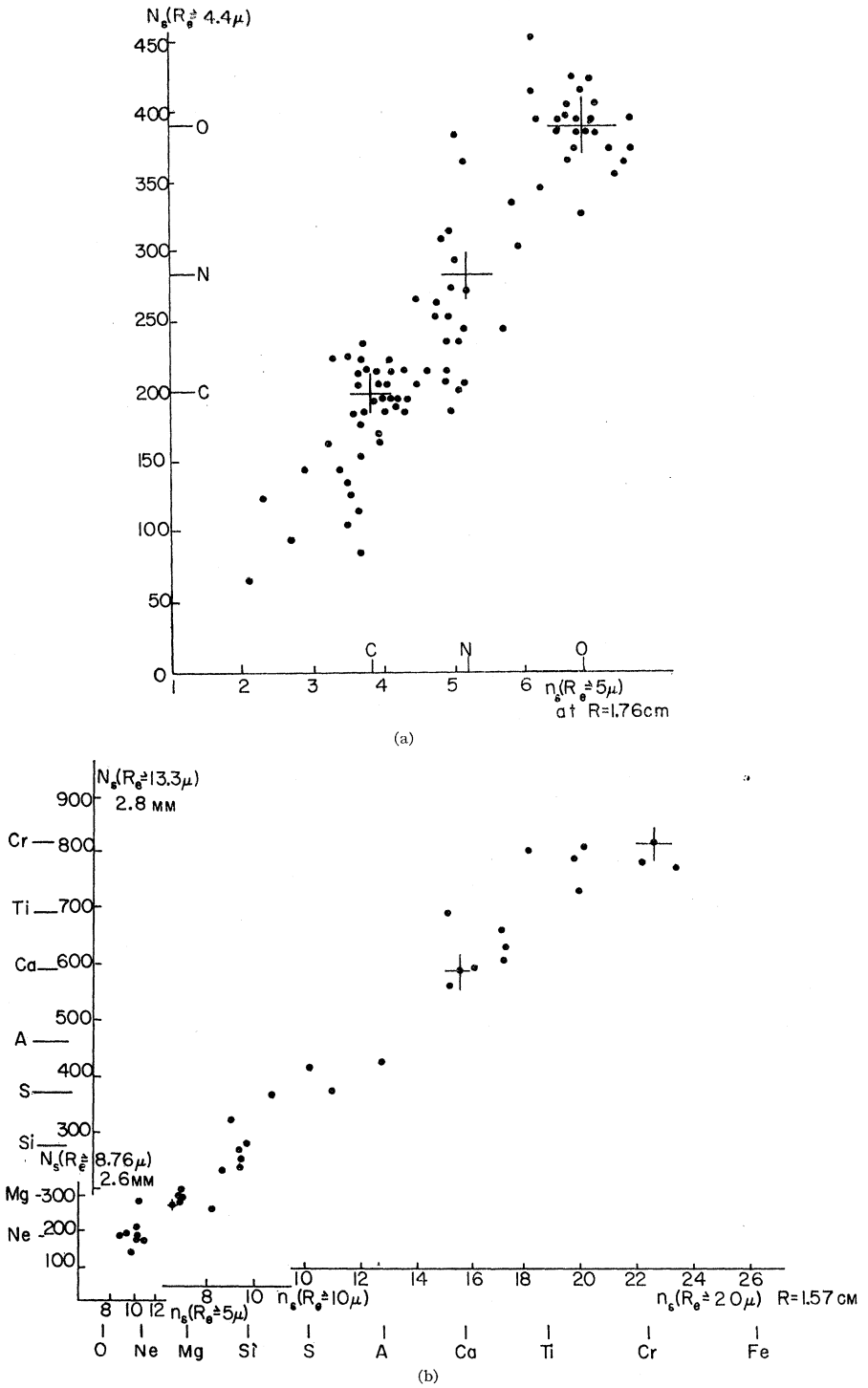

FIG. 1. (a) and (b). Diagrams showing the mutual consistency between the charge determinations by the two methods explained in the text.

formed at the top edge of the stack in order to include all of the particles satisfying the conditions that: (1) the projected zenith angle in the emulsion plane does not exceed 30°; (2) the track length per plate in the zenith direction is larger than or equal to 2.5 mm, or 4.0 mm, when it is traversing the plate in the direction of air-to-glass-surface, or in the opposite direction, respectively; and (3) the ionization is at least that of a relativistic boron nucleus. These conditions are the same as in the supplementary scanning for the stopping C, N, and O nuclei. This result has been partly used in Fig. 10 of Part I to show the shape of the spectrum below the

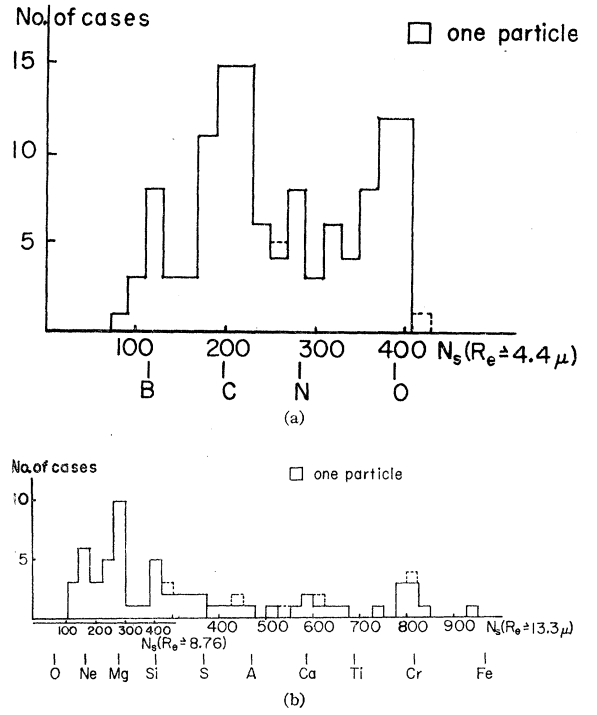

FIG. 2. (a) and (b). Histograms showing the results of the charge determination by the N_δ method. See text.

maximum. The condition (2) is to correct for the overall tilting of the stack at the top edge. All the tracks thus located have been traced until the particles stop, interact, or leave the stack. Only the stopped particles have been used for the later analysis.

The charge of these stopping particles has been identified by the two methods described in detail in Sec. 3 of Part I, one using the integral number, N_δ, of range-cutoff δ rays on the last portion of the ending track and the other using the density n_δ, of range-cutoff δ rays at known residual ranges of the particle. Both methods were calibrated independently. The cutoff ranges of δ rays in the N_δ method are 4.4 μ for $6 \leq Z \leq 8$, 8.8 μ for $8 \leq Z \leq 14$, and 13.3 μ for $12 \leq Z$. The overlapping charge regions have been measured by both schemes in order to assure continuity. The cutoff ranges in the n_δ method are 5, 10, and 20 μ for $6 \leq Z \leq 12$, $12 \leq Z \leq 16$, and $16 \leq Z$, respectively. The same procedure as in the N_δ method has been taken at the overlapping charge regions.

In Fig. 1(a) and Fig. 1(b) are shown the mutual consistencies between the two methods for $6 \leq Z \leq 8$ and for $9 \leq Z$, respectively. The abscissas give the n_δ reduced by the aid of the similarity law explained in Part I, to its value at the residual range of 1.57 cm while the ordinates give N_δ on the last 2.6 mm, or 2.8 mm, of the residual range for $6 \leq Z \leq 14$, or $12 \leq Z$, respectively. The small scatter of the data in the two figures clearly indicates that both methods, each calibrated independently, are quite consistent with each other and that the reliability of both methods is thus greatly increased.

Besides the results on the heavier nuclei of $Z \geq 9$, we report here also the complete results of the supplementary scanning and analysis of the stopping C, N, and O nuclei, a part of which has already been used in Fig. 10 and Table I of Part I.

The results of the charge identification by the N_δ method are shown in Figs. 2(a) and 2(b) for the charge groups of $6 \leq Z \leq 8$ and $9 \leq Z$, respectively.

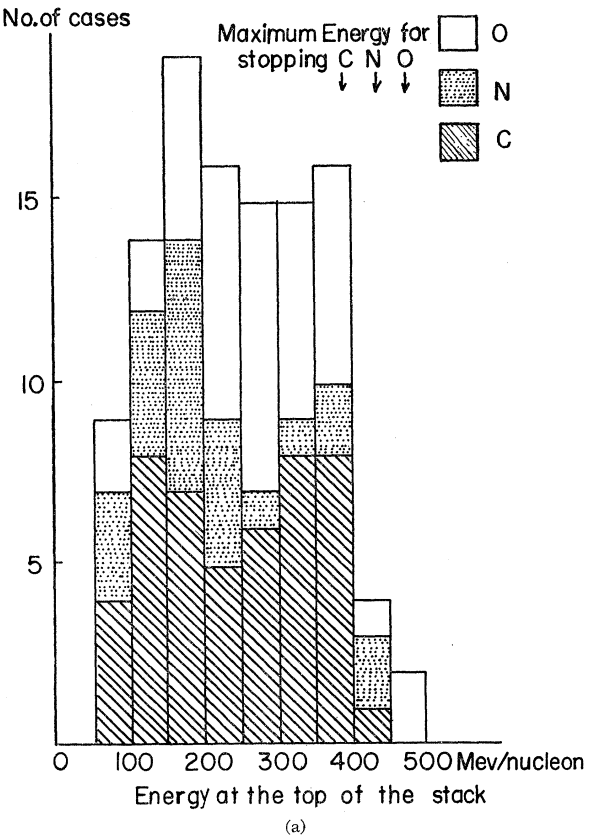

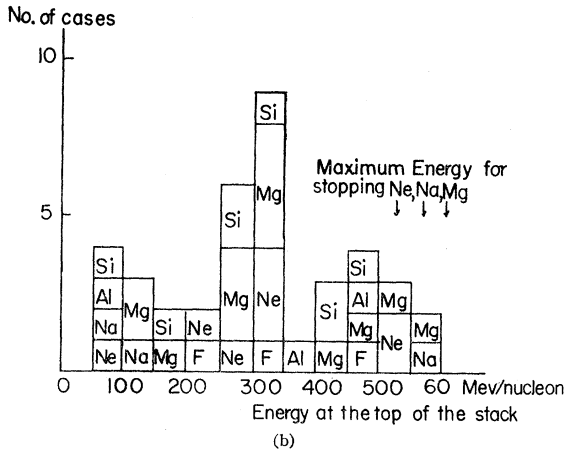

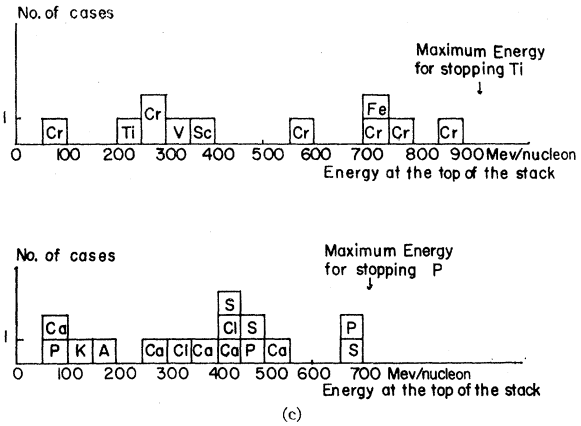

FIG. 3. (a), (b), and (c). Histograms showing the observed numbers of various nuclei with specified energies at the top of the stack.

The energies of the charge-identified particles have been determined from their ranges in the emulsion. The histograms shown in Figs. 3(a), 3(b), and 3(c) give the numbers of observed particles with energies, measured at the top edge of the stack, as indicated in the abscissas for the charge groups of $6 \leq Z \leq 8$, $9 \leq Z \leq 14$, and $15 \leq Z$, respectively.

In order to obtain the energy spectra at the flight altitude, we have to make the correction to account for the collision losses in the stack; the application of this gives us the differential energy spectra at the nominal air depth of 7.6 g/cm² of $M(6 \leq Z \leq 8)$, $H(9 \leq Z \leq 14)$, and $VH(15 \leq Z)$ as shown in Fig. 4. In the figure the abscissa gives the energy per nucleon at the above given air depth and the ordinate is in unit of particles/m² sec sr. Mev.

The extrapolation of these differential energy spectra to those at the top of the atmosphere has been carried out in the following manner. The most accurate method would naturally be to solve the diffusion equation with energy loss, but in view of the small amount of matter traversed by the particles before they are observed in the stack, we can divide the extrapolation into two steps. That is, starting from the observed energy spectrum, $N(E)$, at the flight altitude, we first obtain a fictitious spectrum, $N(E_0)$, which, being corrected only for the energy loss due to ionization, would be observed at the top of the atmosphere if the fragmentation of the nuclei had not occurred at all. We then make the fragmentation correction on this $N(E_0)$ to obtain finally the energy spectrum at the top of the atmosphere, $N_0(E_0)$.

In other words, we assume that all the fragmentation processes have occurred at the very top of the atmosphere and that the secondary particles were the ones that suffered the ionization losses in the air. The difference in the final result of $N_0(E_0)$ from the other choice of the fictitious intermediate spectrum, i.e., $N_0(E)$ instead of $N(E_0)$, is shown in our case to be negligibly small.

In the actual procedure, the individual tracks of Figs. 3(a), 3(b), and 3(c) have been corrected for the energy losses due to the material above the top of the vertical stack which has been estimated to be equivalent, with respect to ionization losses, to 2.65 cm of G-5 emulsion. The elongation of the path length due to the finite zenith angle has been taken into account in each individual case. The corrections due to the fragmentation have been applied to the result thus obtained by using the fragmentation probabilities as given by the averages of Bristol[2] and Chicago[3] data as well as the interaction mean free path as given by Bristol.[2] The nominal air depth for the purpose of this correction has been estimated to be 7.6 g/cm².

The differential energy spectra at the top of the atmosphere obtained in this way are shown in Fig. 13 for M, H, and VH groups. The results are shown also in a tabular form in Table I. The flux values of the C, N, O group above 500 Mev per nucleon have been taken from the results of Part I. Another remark is necessary concerning Fig. 13 or Table I; i.e., the energy range of

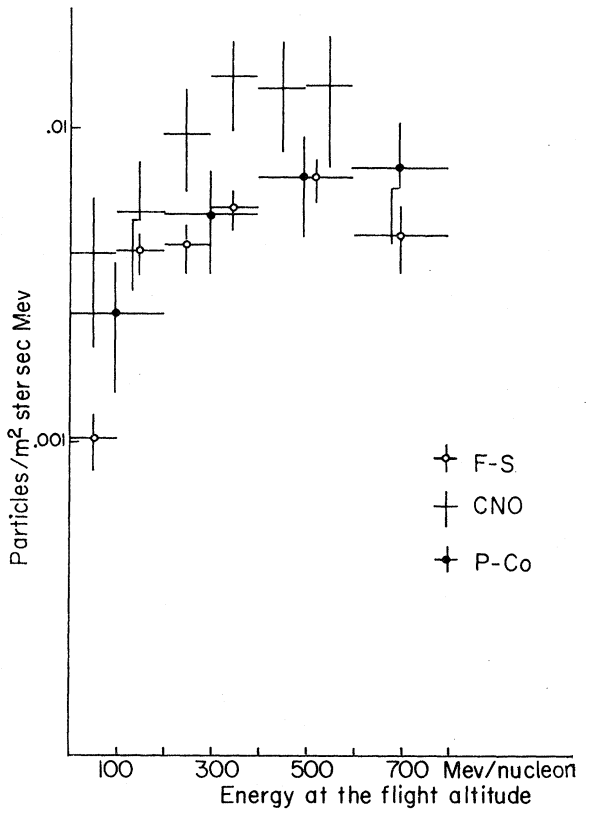

FIG. 4. The differential energy spectra of various charge groups at the nominal air depth of 7.6 g/cm².

[2] P. H. Fowler, R. R. Hillier, and C. J. Waddington *et al.*, Phil. Mag. **2**, 293 (1957).
[3] M. Koshiba, G. Schultz, and M. Schein, Nuovo cimento **9**, 1 (1958).

TABLE I. The differential fluxes at the top of the atmosphere (September 11, 1957, Prince Albert Stack) in unit of particles/m² sec sr 100 Mev. See Fig. 13.

	0	100	200	300	400	500	600	700	800	900	1000 Mev/nuc.
Li Be B		0.07±0.04	0.14±0.05	0.32±0.07	0.42±0.08	0.42±0.08	0.22±0.06				
C N O		0.25±0.18	0.51±0.08	0.71±0.11	0.91±0.14	0.96±0.18		0.63±0.15		0.33±0.11 from $E^{-1.4}$	
F−Si				0.16±0.04	0.23±0.06	0.15±0.06	0.14±0.09				
$15 \leqq Z \leqq 26$					0.11±0.05		0.15±0.04		0.08±0.04		

CNO($E \geq$ 400 Mev) =7.7±0.7 particles/m² sec sr; CNO($E \geq$ 800 Mev) =4.6±0.5 particles/m² sec sr

the particle to arrive at and to stop in the stack is different for different charges and hence, when nuclei of several different charges are treated as a group, a correction is needed at both ends of the observed energy range to account for the fact that there are some of the group members which are observable while others are not. The corrections for this effect have been made by using the observed relative abundances within the group in the energy range where all the group members are observable.

The relative abundance of each individual element at the top of the atmosphere has been obtained in the following manner. We divide the whole elements into four groups of $6 \leq Z \leq 8$, $9 \leq Z \leq 14$, $15 \leq Z \leq 20$, and $21 \leq Z$. We then obtain the relative intensity ratio at the top of the atmosphere of the neighboring charge groups in the energy region where both groups overlap. The relative abundance of individual elements in a group are then determined in the energy range where all the member elements of this group are observable. The results are summarized in Table II where the relative abundances at the top of the atmosphere are shown in terms of the integrated particle number/m² sec sr over the energy range from 200 to 700 Mev per nucleon.

2. THE LIGHT ELEMENTS, Li, Be, AND B

The scanning for the light elements has been made in the same way as described in Sec. 1 for the heavier elements, except that the ionization requirement here was six times minimum or more. This scanning was done in 92 plates without recourse to the previous scanning for the heavier elements. Comparing the results of these two independent scannings, the scanning efficiency was found to exceed 97% for tracks of ionization greater than that of relativistic boron.

Different analysis procedures were taken for stopping, going-through, and interacting particles. The stopping boron and beryllium were identified by the N_δ method and, when it was long enough, by the n_δ method, both described in Part I. The stopping lithium was looked for among a large background of stopping α particles. The method of the calibrated blob density, G_0, was employed and revealed no case of stopping lithium among more than 200 measured cases of apparent α stoppings. The energies of two berylliums and four borons thus found have been estimated from their ranges.

The "through" particles render a more difficult problem. First of all, we have to separate fast lithiums from slow, 200 to 300 Mev per nucleon, α particles. This was achieved by measuring their ionizations at both entrance and exit points. The measurements were done 1 cm inside from the edge so as to avoid the variation of the development near the edges. That is, the ionization of a "through" particle was measured at two points separated, for vertical incidence, by 8 cm from each other. The gap density G_1 of gaps greater than 1 μ was taken as the measure of ionization. A number of well-identified α particles have been used for construction of a calibration curve for this quantity; see Sec. 3. All the ionization measurements were converted to the equivalent α-particle range by means of this calibration curve. Figure 5 gives the results of such measurements. The lithium curve in the figure was obtained from Barkas'[4] table. The lithium tracks thus separated, including the borderline cases, were subjected to the more detailed analysis by measuring the Fowler-Perkins coefficient g. The "through" borons and berylliums have been separated from carbons by means of the calibrated G_0 and/or of the 4-grain δ-ray density. The G_0 has been calibrated by using high-energy Be $\rightarrow 2\alpha$, C $\rightarrow 3\alpha$, and O $\rightarrow 4\alpha$, and was corrected for plate to plate variation. In Fig. 6 is shown the interconsistency of both methods applied on the same track. A counting of 100 blobs or δ rays was made in each measurement.

TABLE II. Integrated fluxes of elements at the top of atmosphere ($200 \leq E \leq 700$ Mev/nucleon) in unit of particles/m² sec sr.

α	Li	Be	B	C	N	O	F	Ne	Na	Mg	Al	Si
44.7±5.8	0.30±0.06	0.55±0.10	0.89±0.14	1.70±0.25	0.85±0.18	1.33±0.22	0.08±0.05	0.16±0.06	0.03±0.03	0.32±0.09	0.08±0.05	0.16±0.06
					3.89±0.34					0.82±0.13		

P	S	Cl	A	K	Ca	Sc	Ti	V	Cr	Mn	Fe
0.05±0.03	0.07±0.04	0.05±0.03	0.02±0.02	0.02±0.02	0.12±0.05	0.04±0.04	0.04±0.04	0.04±0.04	0.15±0.08	···	···
		0.33±0.09						0.27±0.09			

[4] W. H. Barkas, University of California Radiation Laboratory Report UCRL-ZN-991-Rev (unpublished).

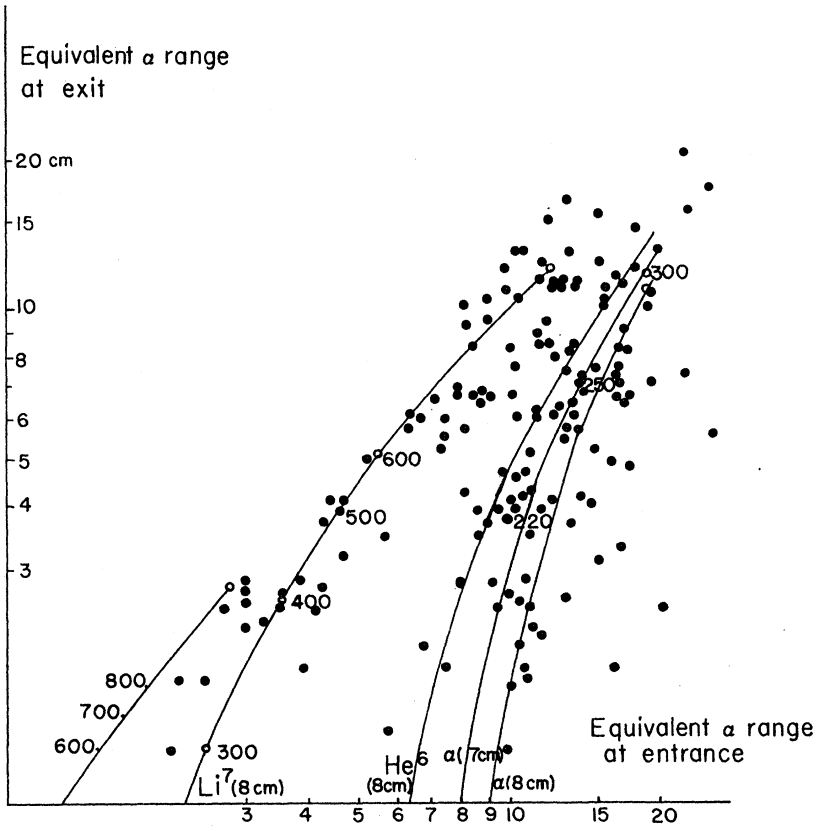

FIG. 5. Separation of fast "through" lithium from slow "through" α particles. See text.

The interaction particles have been analyzed by measuring both the 4-grain δ-ray density of the primary in the vicinity of the interaction and the blob densities of the breakup protons in the forward direction. The separation of slow borons, about 400 Mev per nucleon, from high-energy carbons is shown in Fig. 7 where each point represents the counting of 100 δ rays and 200 blobs. The borderline cases were subjected to more counting of δ rays before they were finally identified as to their charge. The energies of identified boron interactions have been estimated from the measured δ-ray densities. The separation of lithium interactions from slow, 2~300 Mev, α interactions has been accomplished by counting G_1 of primary particles and G_0 of second-

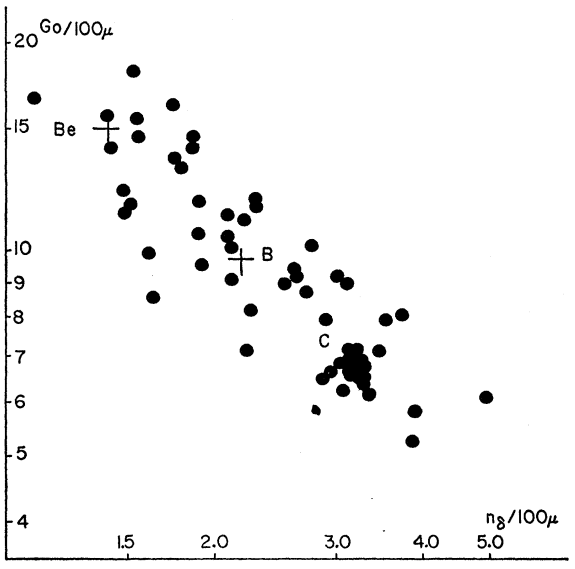

FIG. 6. Consistency check of the two methods of ionization measurement, G_0 and n_δ. See text.

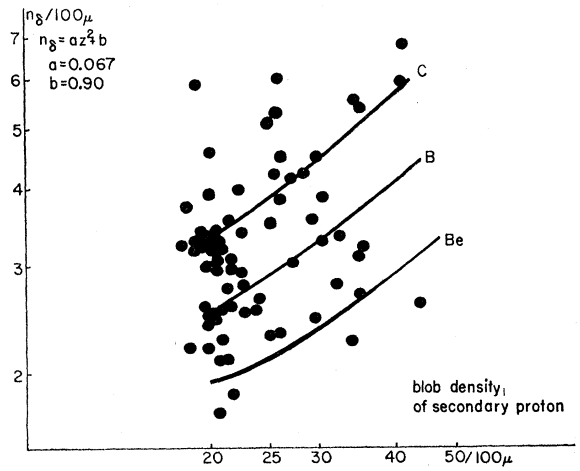

FIG. 7. Separation of boron interactions from carbons.

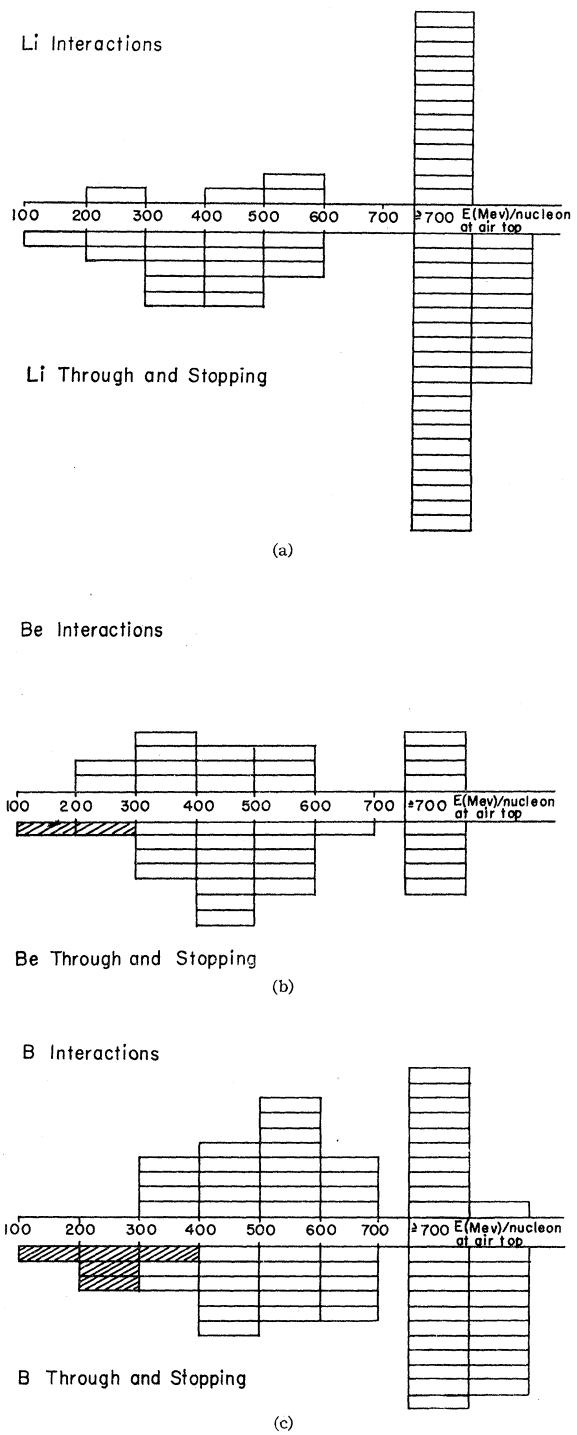

FIG. 8. Histograms of identified lithium (a), beryllium (b), and boron (c).

aries. This is much easier than the separation of borons from carbons.

Figures 8(a), 8(b), and 8(c) give the results of these analyses on lithium, beryllium, and boron, respectively.

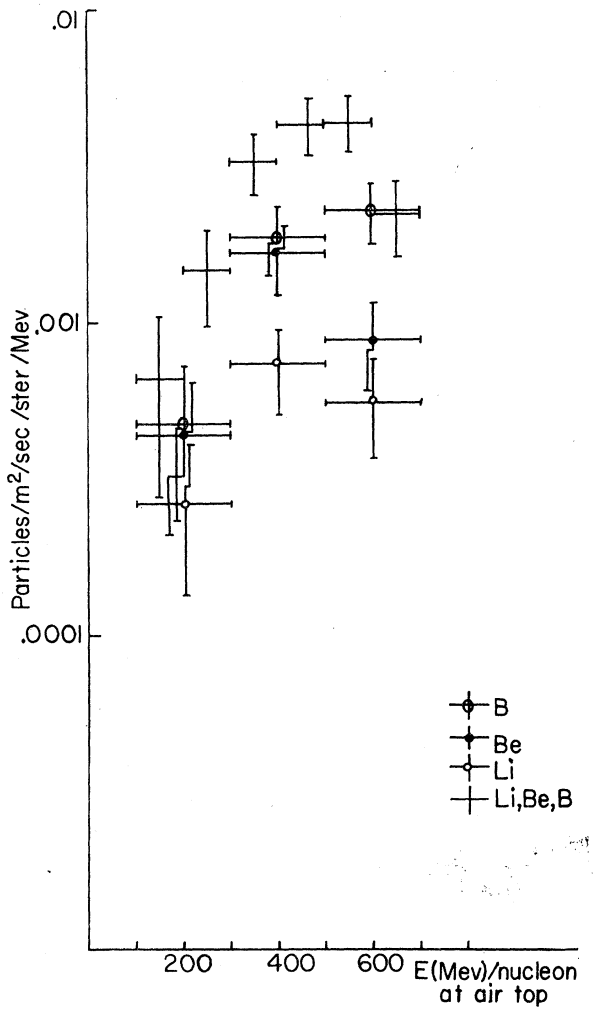

FIG. 9. Energy spectra at the top of atmosphere of lithium, beryllium, boron, and their sum.

Each rectangle signifies one particle. Because of the different methods employed, the interaction cases and the "through" plus stopping cases were shown separately. One can see the general consistency of the results between the two categories. Furthermore, the numbers of cases in the two categories are in agreement with the estimated interaction mean free path in emulsion of these nuclei.

The energy spectra of lithium, beryllium, and boron have been constructed from Fig. 8 by allowing for the fragmentations in the air above 7.6 g/cm², and are shown in Fig. 9, where the sum of the three, the energy spectrum of light elements, is also shown. One can easily see the general resemblance of these spectra to those obtained in Sec. 1 for CNO group and for the heavier elements; i.e., the existence of a broad maximum at around 500 Mev per nucleon and a gradual decrease toward lower energies.

3. ALPHA PARTICLES

The significance of our measurements on the α component can be stated as follows:

(1) So far no attempt seems to have been made to measure the intensities of all the primary components in the charge region from $Z=2$ to $Z\sim 26$ in one and the same stack.[5] It would therefore be of special importance to compare the total flux value and the differential energy spectrum of the α particles with those of the heavier nuclei already obtained in this work.

(2) There have been several measurements of the α component during the periods of different solar activities.[6–8] Therefore, it would be quite interesting to compare our results with these previous ones, for it would cast some light on the effects of solar modulation on the primary cosmic rays.

The cutoff energy, appropriate to the nominal geomagnetic latitude, imposed upon α particles at our place of exposure is 90 Mev/nucleon. Incidentally, the air ionization cutoff for α particles was also 90 Mev/nucleon.

The scanning was made in 8 plates on the middle 10 cm along the line which runs 5 mm below the top edge and parallel to it.

In most of the plates a magnification of 10×10 was used; for checking, the rest of the plates were scanned under 10×20. Neither the recorded tracks nor the α tracks showed any substantial difference in number in either case.

The following scanning criteria were adopted:

(1) The ionization was to be greater than 2.5 minimum. More specifically, the number of gaps longer than 1.8 μ were counted for a length of 270 μ of each track and the tracks with less than 20 gaps were accepted.

(2) The projected length in each plate was to be greater than 6 mm. In actual cases, to make allowance for the systematic tilting of the emulsion at the top edge, the following convention was used: The projected length in scanned area of the plate was to be greater than 5 mm for the tracks leaving the emulsion at its glass surface and greater than 8 mm for those leaving at its air surface.

(3) The zenith angle was to be smaller than 30°. The tracks having an interaction in the scanned plate within 2 cm of its top edge were rejected without recording, as were those ending in the scanned plate and having ionization which enabled us to distinctly identify them as p or d.

The other tracks satisfying the scanning criteria were recorded and traced until they ended in the emulsion, suffered large-angle scatterings, made an interaction, or left from the bottom edge. Those which interacted within 8 cm of the top edge were rejected from the later measurement.

It is true that one can use the combination of the scattering measurement with the ionization measurement near the top edge to separate genuine α particles from slow protons or deuterons and can use the ionization as the measure of the α-particle energy.

The reason why we preferred the more painstaking method described above is that we wished, first, to secure greater certainty in the track identification and, second, to measure the ionization of the identified α tracks at a place as distant as possible from the top edge.

Deuterons and tritons of energy $\sim$100 Mev per nucleon have ionizations equal to that of $\sim$1-Bev α particles. Their second differences $\bar{D}(500\,\mu)$ in multiple scattering measurements are:

$$\bar{D}(500\,\mu)\sim 1.34\,\mu \text{ for 100-Mev deuterons,}$$
$$\sim 0.93\,\mu \text{ for 100-Mev tritons,}$$
$$\sim 0.35\,\mu \text{ for 1-Bev } \alpha \text{ particles,}$$

respectively, where the scattering constant is taken to be $\sim$25 and the spurious scattering of $\sim 0.3\,\mu$ due to various noises has been taken into account.

Naturally, this can give a good separation if the fluxes of deuterons and tritons are much smaller than that of α particles. However, we do not have any reliable data on deuterons and tritons at present. If the numbers of deuterons and tritons of energy $\sim$100 Mev per nucleon are n_d and n_t, respectively, then the numbers of deuteron and triton tracks with values of $\bar{D}(500\,\mu)$ which fall within one standard deviation of that of $\sim$1-Bev α particles are 3.5% of n_d and 9.5% of n_t, respectively. Hence the "scattering-ionization method" is not completely free from the danger of including the contaminating deuterons and tritons, if their fluxes are not small compared to that of the α particles.

On the other hand, if one traces the tracks to the place 6.5 cm from the top edge, a 100-Mev deuteron will stop, and a triton of the same energy will stop after traversing 9.5 cm of emulsion. Obvious large-angle deflections by multiple scatterings will show up in even shorter distances. The method we have adopted is, therefore, the one which leaves no ambiguity whatsoever in track identification.

The scanning in 8 plates yielded 184 α particles, 25 heavier nuclei, 230 contaminating protons and deuterons, and 11 particles which interacted within 8 cm of the top edge.

---

[5] Except for two: One is the well-known work by H. L. Bradt and B. Peters [Phys. Rev. **80**, 943 (1950)]. To our regret, their work shares the common defect with most other pioneer works in that their statistics are not sufficient. Furthermore, they lacked the means which would have enabled them to treat the problem of the differential energy spectra. The other is the measurement by A. Engler, M. F. Kaplon, and J. Klarmann. Their flight, however, was carried out at 41° N geomagnetic latitude so that the determination of the differential energy spectra were out of their scope.

[6] P. H. Fowler, C. J. Waddington, P. S. Freier, J. Naugle, and E. P. Ney, Phil. Mag. **8**, 157 (1957).

[7] F. B. McDonald, Phys. Rev. **107**, 1386 (1957); Suppl. Nuovo cimento **8**, 500 (1958).

[8] P. S. Freier, E. P. Ney, and P. H. Fowler, Suppl. Nuovo cimento **8**, 492 (1958); Nature **181**, 1319 (1958).

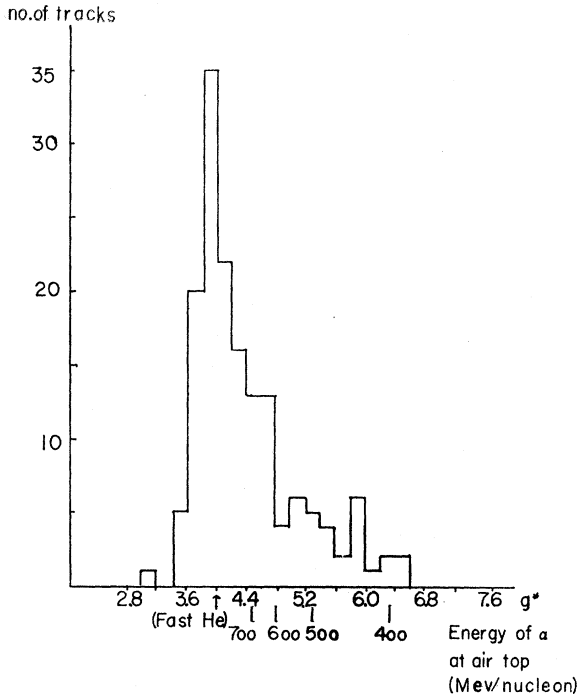

FIG. 10. Ionization distribution of α particles with $g^* \lesssim 6.4$ at 1.5 cm above the emulsion bottom. Tracks with $g^* \gtrsim 6.4$ are measured by the method which does not use g^* as the measure of ionization. For the details, see the text.

The measurement of the ionization of the identified α tracks were performed in the following way:

(1) For tracks which ended in the emulsion, the energy has been determined from the range in the emulsion.

(2) For particles which left from the bottom edge and those which interacted at places more than 8 cm deep from the top edge, the ionization measurement on the track was made at a place 1 to 3 cm from the bottom edge.

The reason that we adopted the latter way of measurement for the "nonstopping" alphas is that we wished to attain a greater precision in energy determination.

TABLE III. Comparison of ionization measurements on α particles at the top and the bottom of the stack.

Energy of α at top of atmosphere (Mev/nucleon)	Energy of α 1.5 cm from emulsion top (Mev/nucleon)	Corresponding ionization I/I_0	Energy of α 1.5 cm from emulsion bottom (Mev/nucleon)	Corresponding ionization I/I_0
800	770	4.2	730	4.3
700	670	4.4	630	4.5
600	570	4.6	520	4.8
500	570	5.0	420	5.3
400	370	5.7	310	6.3
300	260	6.9	190	8.4
250	210	8.0	110	12.3

In particular the necessity of a high degree of precision will be keenly felt in measuring higher energies, when one considers that about half of all the α particles have relativistic ionizations.

The α particles lose their energy by ionization in traversing emulsion, so that their energies per nucleon will be 40 Mev to 120 Mev lower at the place 1.5 cm from the bottom edge than at the place 1.5 cm from the top edge. The energy loss is a function of their incident energy at the top of the emulsion.

The lower the energy of an α particle, the more precise is its determination, because dI/dE increases with decreasing energy. Therefore it can be seen that the place near the bottom will be more advantageous for the purpose of primary energy measurements.

In Table III one can see how much greater precision is attainable by the measurement near the bottom edge than near the top edge of our stack.

The ionization measurement was made by counting blobs and gaps.

First we have to determine what minimum gap length is to be used to obtain the best resolution in determining the ionization.

Let g and G_l designate the Fowler-Perkins coefficient and the number per unit length of gaps longer than l, respectively, of the track under consideration. The larger the value of l the more sensitive will be the variation of G_l to that of g. Let ΔG_l be the variation of G_l corresponding to the variation Δg of g. If we assume that for smaller values of g the relation

$$G_l = g e^{-g(l+\alpha)}$$

holds, then the relative sensitivity S of G_l with respect to the variation of g is given by

$$\begin{aligned} S &\equiv |\Delta G_l/\Delta g|/G_l \\ &= |l+\alpha-(1/g)|. \end{aligned}$$

On the other hand, larger values of l will result in smaller numbers of gaps on a given track length L, and hence the statistical error in G_l will become larger. Let the relative statistical error be N, given by

$$N \equiv (G_l L)^{-\frac{1}{2}}.$$

Thus the value of l which corresponds to the optimum $S-N$ ratio, l^*, will be given by the condition

$$\frac{\partial}{\partial l}(S/N)=0, \quad \text{or} \quad l^*=(3/g)-\alpha.$$

Therefore, different values of l should be adopted for different values of g in order to get the best possible resolution.

For $g^* \lesssim 6.4$ the method of the Fowler-Perkins coefficient using blobs and gaps longer than 2 μ was applied, where $g^*=g/g_0$ and g_0 is the Fowler-Perkins coefficient for relativistic electrons.

For each track 400 blobs and 100 gaps were counted. To minimize the effect of emulsion depth on the measurement of g, $\frac{1}{6}$ of the track has been discarded at both ends.

For $g^* \lesssim 6.4$, precision in the g determination is particularly necessary. For these values of g^*, the variation arising from the nonuniformity of the development between different plates or between different places in the same plate was shown not to exceed 5% in the blob density and 10% in the gap density.

The relative error in g is given by

$$\left|\frac{\Delta g}{g}\right| = \frac{1}{gl}\left\{\frac{(\Delta_n B)^2+(\Delta_d B)^2+(\Delta_s B)^2}{B^2} + \frac{(\Delta_n G)^2+(\Delta_d G)^2+(\Delta_s G)^2}{G^2}\right\}^{\frac{1}{2}},$$

where the notations are as follows: l=minimum gap length adopted; B=total number of blobs counted; $\Delta_n B$=statistical error in B; $\Delta_d B$=fluctuation in B arising from the nonuniformity of development; $\Delta_s B$ =subjective errors in B; G, $\Delta_n G$, $\Delta_d G$, and $\Delta_s G$ are the corresponding quantities for gaps.

Substitution of the values:

$$gl=2,$$
$$\Delta_n B/B=5\%, \quad \Delta_d B/B \lesssim 5\%, \quad \Delta_s B/B<5\%,$$
$$\Delta_n G/G=10\%, \quad \Delta_d G/G \lesssim 10\%, \quad \Delta_s G/G \lesssim 10\%,$$

gives

$$|\Delta g/g| \lesssim 10\%.$$

Incidentally, values of g greater than $4.8g_0$ can be recognized as meaningfully different from the relativistic g's.

The ionization distribution of α particles with $g^* \lesssim 6.4$ at the emulsion bottom is shown in Fig. 10.

In translating these values of g^* into the energy scale, the range-ionization curve given by Barkas[4] is used and it is assumed that g is proportional to the ionization.

If the error in g^* is 10%, the precision in the energy determination of α particles at air-top may be estimated as shown in Table IV.

TABLE IV. Estimated error in the α-particle energy resulting from a 10% error in g^* measurement. See text.

Energy of α at top of atmosphere (Mev/nucleon)	Error in energy (Mev/nucleon)
350	$\begin{cases}+50\\-30\end{cases}$
450	$\begin{cases}+90\\-50\end{cases}$
550	$\begin{cases}+140\\-80\end{cases}$

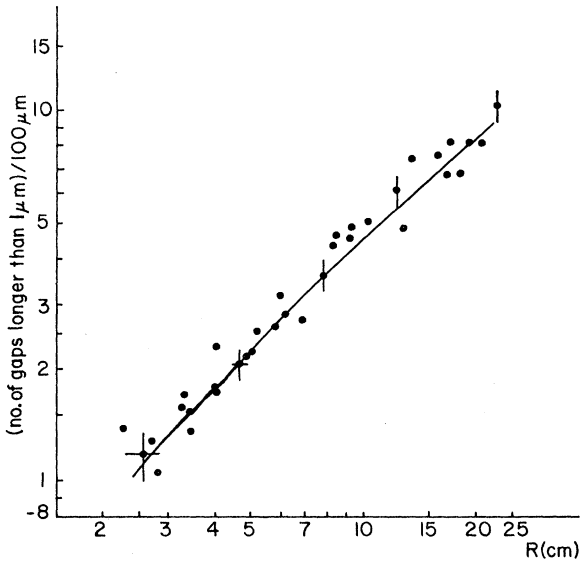

FIG. 11. The empirical curve which gives the relation between the residual range R and the gap density G_1, the number per 100 μ of gaps longer than 1 μ, for α particles. Vertical bars represent the statistical errors of G_1. Each point at $R>4$ cm and at $R<4$ cm corresponds to 100 and 50 gaps, respectively.

For $g^* \gtrsim 6.4$, gaps longer than 1 μ were counted, but, as saturation sets in and the proportionality of g to ionization no longer holds, it would not be permissible to use the Barkas curve in converting g^* into energy. Therefore the ionization measurement was made by using the gap density G_1 alone and an empirical relation between G_1 and the residual range R was constructed. The points beyond $R \geq 10$ cm have been obtained by adding the data of the slow through particles to those of the stopping ones.

The empirical curve thus obtained is shown in Fig. 11. The number of gaps counted is 100 for each point in the plot. It can be seen from the figure that both the subjective errors and the fluctuations arising from the nonuniformity of development are within the statistical error.

The residual ranges of alphas can now be determined and they are converted into energy using the range-energy relation given by Barkas.[4]

If an error of 20% in G_1 is assumed, the corresponding error in the energy determination of alphas at the top of the atmosphere may be estimated as shown in Table V.

The correction to the α flux for the interactions in emulsion has been made using the interaction mean free

TABLE V. Estimated error in the α-particle energy resulting from a 20% error in G_1. See text.

Energy of α at top of atmosphere	250	300	350
Estimated error in this energy (Mev/nucleon)	±10	±20	±30

TABLE VI. Correction to the α-particle flux for the fragmentations of heavier elements in the residual air.

Energy of α at top of atmosphere (Mev/nucleon)	Correction
100–200	2.0%
200–300	3.5%
300<	4.0%

path in G-5 of $\lambda=(19.9\pm1.2)$ cm, obtained from the values given by Quareni,[9] Waddington,[10] and Engler.[11]

The correction for the interactions with the atmospheric nuclei was made using the interaction mean free path in air of[12] $\lambda=50$ g/cm^2.

The number of secondary α particles arising from the fragmentations of the heavier nuclei was estimated using the interaction mean free paths and the fragmentation probabilities given by Fowler,[2] Koshiba,[3] and Rajopadhye,[13] and has been subtracted.

The corrections from these sources are shown in Table VI. The corrections from other sources have been neglected.

The flux values obtained for each energy interval are shown in Table VII, and the differential energy spectrum in Fig. 12. As can be seen from Tables III and IV, the energy determination is meaningful only for $E\leq600$ Mev, so that in the figure for $E\geq600$ Mev the points are plotted which are calculated assuming the following shape of the integral energy spectrum:

$$N(>E)\propto(1+E)^{-1.4},\quad (E \text{ in Bev})$$

which is based upon the data obtained by other workers[12] and the observed integral flux value of

$$N(>0.6)=96.5\pm8.5 \text{ particles/m}^2 \text{ sec sr}.$$

For the energy region 160 Mev to 200 Mev an additional result with improved statistics of stopping particles has also been plotted in Fig. 12.

The comparison of the α flux with that of C, N, O nuclei is given in Table VIII.

TABLE VII. The α-particle flux values.

α energy at top of atmosphere (Mev/nucleon)	100–200	200–300	300–400	400–600	600<
α flux (particles/m^2 sec sr)	3.8 ± 1.6	9.0 ± 2.6	5.2 ± 2.0	22.4 ± 4.1	96.5 ± 8.5

Total flux of α with energies >200 Mev/nucleon at top of atmosphere $=133\pm10$/m^2 sec sr

The ratio of C, N, O flux to that of α is somewhat larger than the values given so far by other workers.[11,12,14] In obtaining these values, however, the measurements of C, N, O flux have seldom been done in the same stack that gave the α-particle fluxes.

4. DISCUSSIONS AND CONCLUSIONS

The results obtained in this work, Fig. 13 and Tables I and II, strongly fortify the conclusions of Part I that the energy spectra of different charge groups do have a similar shape, and that there exists a broad maximum at about 500 Mev per nucleon. The spectrum of the light element group seems to show a small deviation from this similarity law and we shall discuss this point further in a later part of this section.

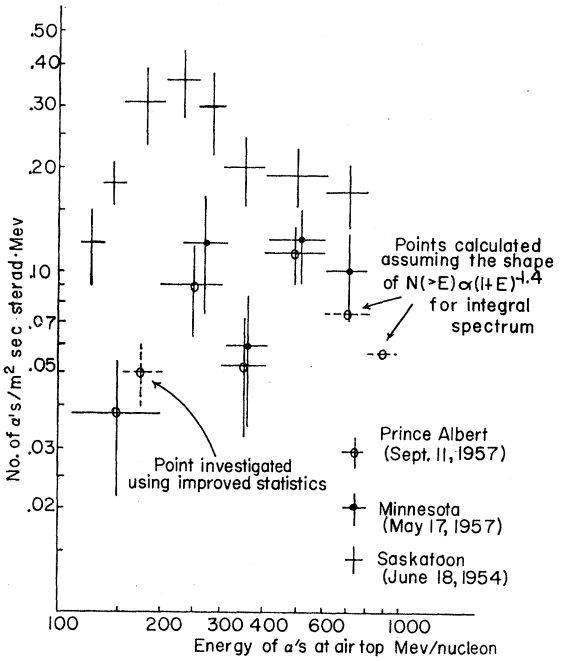

FIG. 12. The differential energy spectrum of α particles. For comparison, the results obtained by Minnesota group in the flight on June 18, 1954, at Saskatoon and in the flight on May 17, 1957, at Minnesota are also plotted in the figure.

This similarity in the spectrum shape suggests that there exists a certain similarity law for the processes responsible for the observed spectral shapes. It seems possible to extend this similarity to include the proton component[15,16] if we use the magnetic rigidity of the particle instead of the per-nucleon energy.

The implication of this similarity law and of the general shape of the spectra has been discussed in detail elsewhere.[16,17]

[9] G. Quareni and G. T. Zorn, Nuovo cimento **1**, 1282 (1955).
[10] C. J. Waddington, Phil. Mag. **1**, 105 (1956).
[11] A. Engler, M. F. Kaplon, and J. Klarmann, see reference 5.
[12] See S. F. Singer, in *Progress in Elementary Particles and Cosmic-Ray Physics*, edited by J. G. Wilson and S. A. Wouthuysen (North Holland Publishing Company, Amsterdam, 1958), Vol. 4, Chap. 4.
[13] V. Y. Rajopadhye and C. J. Waddington, Phil. Mag. **3**, 19 (1958).
[14] Bradt and Peters, see reference 5.
[15] This was clearly indicated, in particular, by F. M. McDonald, Bull. Am. Phys. Soc. **5**, 292 (1960).
[16] S. Hayakawa and M. Koshiba, Progr. Theoret. Phys. (Kyoto) **21**, 473 (1959).
[17] S. Hayakawa, M. Koshiba, and Y. Terashima, *Proceedings of*

We now discuss the light elements. Figure 14 shows the spectra of the primary Li, Be, and B separately, in which all the necessary corrections have already been applied, i.e., for the ionization as well as for fragmentation losses in the residual air. Their flux values are normalized to those of C, N, O nuclei in the corresponding energy range. The results seem to indicate an increase, relative to C, N, O, of the light elements in the energy range of 300 to 700 Mev per nucleon.

As has been described in the preceding section, this cannot entirely be ascribed to the inclusion of relativistic carbons as slow borons. We estimate that this misclassification will not alter the spectrum by more than 10% at the worst, and, hence, the relative increase of fluxes at energies from 300 to 700 Mev per nucleon appears to be real.

The question now is whether this increase is due to the fact that the amount of interstellar matter traversed by these slow particles is actually larger than that traversed by the higher energy ones, or due merely to the energy dependence of the fragmentation probabilities.

Experimental data, though rather scanty, on the energy dependence of the fragmentation probabilities

TABLE VIII. Comparison of α and CNO fluxes.

Energy region (Mev/nucleon)	Flux CNO	Flux α	CNO to α ratio (%)
200–700	3.89±0.34	44.7±5.8	8.7±1.4
800<	4.6 ±0.5	82.0±7.0	5.6±0.9
400<	7.7 ±0.7	119.0±9.0	6.5±0.8

suggest decreasing amounts of Li, increasing amounts of B, and almost equal amounts of Be in the low-energy region as compared with their values in the high-energy region.

Restricting ourselves, however, to the B nuclei for which we have relatively more information concerning the relevant fragmentation probabilities, we find that the main contribution to the production of boron nuclei comes from the reactions:

$$C^{12}+p \rightarrow B^{11}+p+p,$$
$$C^{12}+p \rightarrow C^{11}+p+n, \quad (C^{11} \rightarrow B^{11}+e+\nu).$$

The cross sections of these reactions are known, experimentally and theoretically, to follow the energy dependence of the nucleon-nucleon cross section. Namely, up to around 400 Mev it has a $1/E$ dependence, while beyond this energy region it stays at an approximately constant level.

Therefore, we come to the conclusion that the relative increase of boron at energies from 400 to 700 Mev is actually due to an increased amount of matter traversed

the Moscow Cosmic-Ray Conference, July 6–11, 1959 (International Union of Pure and Applied Physics, Moscow, 1960), Vol. III, p. 181.

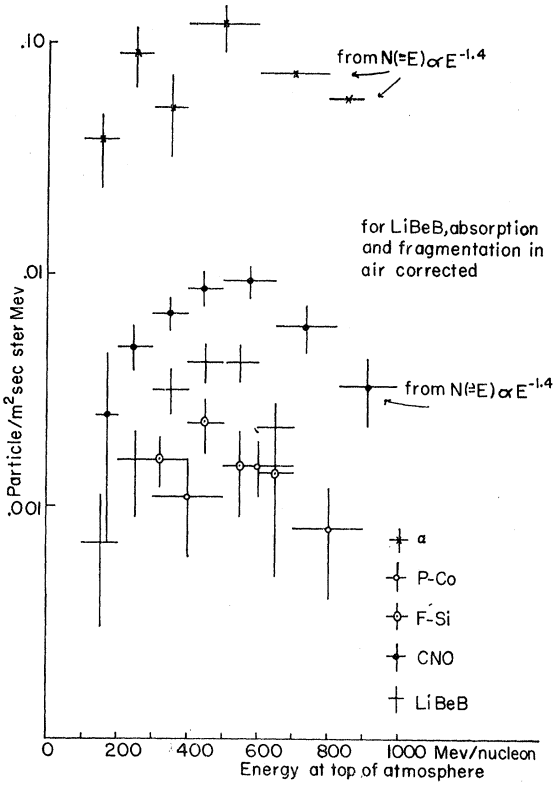

FIG. 13. Energy spectra of various element groups observed at Prince Albert, Canada, on September 11, 1957.

by the parent carbons, and heavier elements, of this energy range. The apparent deviation from this conclusion observed in the energy region below 300 Mev

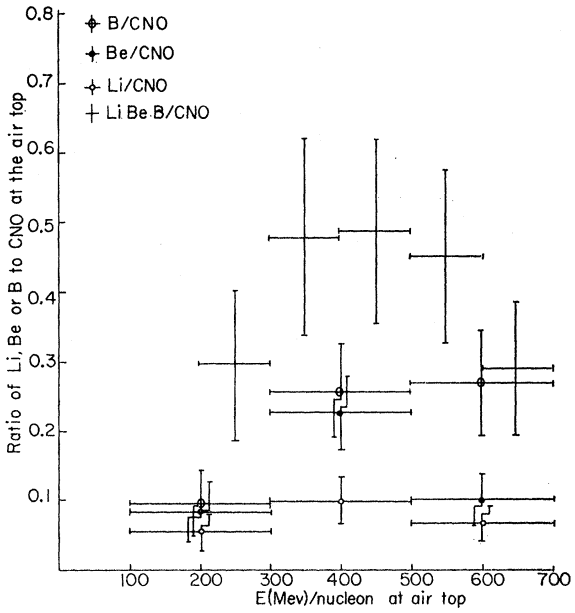

FIG. 14. Abundances of lithium, beryllium, and boron relative to CNO.

TABLE IX. Light-to-medium and heavy-to-medium ratios in low- and high-energy regions.

	This experiment 200–700 Mev/nucleon	Texas experiment 1000 Mev/nucleon
L/M	0.41±0.06	0.32±0.07
H/M	0.38±0.05	0.48±0.10

does not seem a serious objection, because, in addition to the poor statistics of the data in this energy range, the ionization loss is quite substantial at these low energies and our approximate method (i.e., separate corrections for the ionization and the fragmentation) used in extrapolating the observed spectrum, at 7.6 g/cm², to the top of the atmosphere becomes invalid. The same conclusion of an elongated path length for the low-energy particles can be reached qualitatively from the observed Li and Be spectra.

This conclusion, however, has to be checked with respect to the amount of H nuclei destroyed on the increased path length. For this purpose, we compare our results with those obtained for the high-energy region[3] in Table IX.

The nominal amounts of traversed matter are estimated, from the observed L/M values, to be 3 g/cm² and 5 g/cm² for high-energy and for low-energy particles, respectively. These values in turn give for H/M in the region of the source the values 0.64 and 0.58, respectively. The agreement, within the statistical accuracy, of these two values indicates the self-consistency of our tentative conclusion of elongated path lengths for low-energy particles.

This conclusion, however, has to be substantiated by further experiments with better statistics, and more information on the fragmentation probabilities, in particular their energy dependence, is urgently needed in this connection.

Our conclusion can be considered as indicating that the Fermi type of acceleration in interstellar space is ineffective at these low energies compared with the effect of the elongation of path length due to diffusion. Otherwise, the spectra should show the opposite tendency, i.e., the ratio L/M increasing with energy as $\log E$. We might further mention that this result can be regarded as a support for the theory of supernovae origin of cosmic rays together with subsequent diffusion in the galaxies.

Turning now our attention to the abundances of various elements in the primary radiation, Table II, we notice that the abundances observed in the low-energy region are in general agreement, except for the possible small changes just discussed, with those at higher energies reported previously. A fuller theoretical discussion of these results is given by Hayakawa *et al.*[18] Here we merely point out the fact that the relative overabundance of the heavy elements of $Z \gtrsim 9$ with respect to C, N, O and the anomaly in the C:N:O ratio have now been experimentally established in the low-energy as well as in the high-energy region, thereby suggesting that these elements seem to have been synthesized in some extraordinary stages, or at least in some non-equilibrium stage, of stellar evolution.

Looking now at the α component, the comparison of our result with that of the Minnesota group obtained in the flight on May 17, 1957[8] shows a remarkable similarity between the two. While some better statistics are needed to discuss the more detailed features in the shape of the spectrum, at least the following two conclusions could be drawn from our present result:

(1) The total flux of the primary α particles on September 11, 1957 at Prince Albert was about half of that on June 18, 1954, at Saskatoon.

(2) The two energy spectra seem to differ from each other also in shape, in that ours has its maximum at an energy considerably higher than theirs.[17]

Finally, we would like to point out the following conclusion. Namely, there has been no single case of antiparticles among the observed stopping particles of about 500 α particles, 300 (C,N,O), and heavier elements, and more than 1000 singly charged particles. Even with a somewhat larger interaction cross section of antiparticles, this will set an upper limit for the amount of antimatter in the primary radiation at about 0.1%.

ACKNOWLEDGMENTS

We express our thanks to the K. Murakami and T. Yoshizawa for their aid both in scanning and in analysis.

[18] S. Hayakawa, C. Hayashi, K. Ito, J. Jugaku, M. Nishida, and N. Ohyama, see reference 17, p. 171.